Modeling the critical MCOR-causing deletion in mouse unveils aberrant *Sox21* expression in developing and adult iris and ciliary body, and implicates *Tgfb2* in MCOR-associated glaucoma and myopia.

Clémentine Angée [#1], Elisa Erjavec[#1], Djihad Hadjadj[2], Bruno Passet[3], Pierre David[4], Corinne Kostic[5], Emmanuel Dodé[6], Xavier Zanlonghi[6], Nicolas Cagnard[7], Brigitte Nedelec[1], Sylvain Crippa[5], Christine Bole-Feysot[8], Mohammed Zarhrate[8], Johan Castille[3], Jean-Luc Vilotte[3], Patrick Calvas[9], Julie Plaisancié[9], Nicolas Chassaing[9], Josseline Kaplan[1], Jean-Michel Rozet[1]*, Lucas Fares Taie[1]*

1. Laboratory of Genetics in Ophthalmology (LGO), INSERM UMR1163, Institute of Genetic Diseases, Imagine and Université Paris Cité; Paris, France.
2. Institut Cochin, Inserm U1016, CNRS UMR8104, UFR de Pharmacie de Paris, Université Paris Cité, CARPEM; Paris, France.
3. University of Paris-Saclay, INRAE, AgroParisTech, UMR1313 GABI; Jouy-en-Josas, France
4. Transgenesis Platform, Laboratoire d'Expérimentation Animale et Transgenèse (LEAT), Imagine Institute, Structure Fédérative de Recherche Necker INSERM US24/CNRS UMS3633; Paris, France
5. Group for Retinal Disorder Research, Department of Ophthalmology, University of Lausanne, Jules-Gonin Eye Hospital, Fondation Asile des Aveugles; Lausanne, Switzerland
6. Institut Ophtalmologique de L'Ouest-Clinique Jules VERNE; Nantes, France.
7. Université Paris Cité, Bioinformatics Core Facility, Imagine Institute, INSERM UMR 1163; Paris, France
8. Université Paris Cité, Genomics Platform, Imagine Institute, INSERM UMR 1163; Paris, France
9. Centre de Référence pour les Affections Rares en Génétique Ophtalmologique (CARGO), CHU Toulouse; Toulouse, France

# Contributed equally

*Correspondence: lucas.fares-taie@inserm.fr, jean-michel.rozet@inserm.fr

ABSTRACT

Congenital microcoria (MCOR) is a rare hereditary developmental defect of the iris dilator muscle, frequently associated with high axial myopia and high intraocular pressure (IOP) glaucoma. The condition is caused by submicroscopic rearrangements of chromosome 13q32.1. However, the mechanisms underlying the failure of iris development and the origin of associated features remain elusive. Here, we present a 3D architecture model of the 13q32.1 region, demonstrating that MCOR-related deletions consistently disrupt the boundary between two Topologically Associating Domains (TADs). Deleting the critical MCOR-causing region in mice reveals ectopic *Sox21* expression precisely aligning with *Dct*, each located in one of the two neighbor TADs. This observation is consistent with the TADs' boundary alteration and adoption of *Dct* regulatory elements by the *Sox21* promoter. Additionally, we identify *Tgfb2* as a target gene of SOX21 and show TGFB2 accumulation in the aqueous humor of a MCOR-affected patient. Accumulation of TGFB2 is recognized for its role in glaucoma and potential impact on axial myopia. Our results highlight the importance of SOX21-TGFB2 signaling in iris development and control of eye growth and IOP. Insights from congenital microcoria studies may provide therapeutic avenues for this condition but also for glaucoma and high myopia conditions, that affect millions of people.

INTRODUCTION

The iris is a remarkable ocular structure, serving a dual purpose by finely tuning the amount of light that reaches the retina and regulating intraocular pressure (IOP). It comprises a stroma, a double epithelium layer and two dynamic muscles, the dilator and the sphincter, that work together to adjust the size of the pupil and hence the light intensity for optimal vision. The iris is rooted to both the corneal-scleral junction and the ciliary body (CB), whose stroma and epithelial layers are continuous with those of the iris. This structural arrangement creates an open space known as the irido-corneal angle where the aqueous humor (AH) produced by the CB to nourish ocular tissues is drained out, playing a vital role in maintaining intraocular pressure (Davis-Silberman and Ashery-Padan 2008). An increase in IOP is a prominent risk factor for optic nerve damage and glaucoma (GLC) (Gould et al. 2004).

Congenital microcoria (MCOR, MIM#156600) is an extremely rare autosomal dominant condition affecting both of these functions. It is characterized by the partial or complete absence of the iris dilator muscle, which normally originates from the anterior part of the epithelial layer (AEL) and extends along its stroma. The sphincter muscle near the pupil's edge retains full functionality. The absence of dilator muscle fibers is evident in the presence of pinhole-sized pupils (< 2mm) that exhibit minimal or no dilation, even when mydriatic drugs are used. This also leads to the iris thinning and atrophy of the stroma, particularly in the dilator muscle region, which permits light to pass through, inducing iris transillumination (Simpson and Parsons 1989; Ramirez-Miranda et al. 2011). In the vast majority of the cases, this abnormal development of the iris does not affect the chamber angle that is wide-open although prominent iris processes and a higher insertion of the iris root in the angle have been typically described. Alongside dilation problems, individuals with MCOR are at a substantially increased risk of developing high axial myopia, affecting 70% of cases. Among those with high myopia, half also experiences juvenile-onset high IOP glaucoma, an unusually high prevalence compared to the general population, which stands at 34% of all MCOR cases (reviewed in Angée et al. in 2021). The underlying causes of these associated features is highly debated. It was suggested that the tendency to close the eyelids to reduce the glare caused by iris transillumination in MCOR could lead to form-deprivation myopia. However, the absence of a clear link between myopia and oculocutaneous albinism, which shares similar symptoms of iris transillumination and light sensitivity, challenges this notion (Angée et al. 2021). In relation to glaucoma, high axial myopia, a known contributor to the condition, and the anatomical features of microcoric chamber angles, which may affect AH flow, may play a contributory role but are not solely

sufficient. This is evident from the fact that although all individuals with glaucoma exhibit these anomalies, only about a third of those with these anatomical variations actually develop glaucoma.

The disease was ascribed to submicroscopic rearrangement of chromosome 13q32.1, particularly deletions and a reciprocal duplication, suggesting that the disease is linked to an alteration of the regulatory landscape of the region (Fares-Taie et al. 2015; Sergouniotis et al. 2017; Pozza et al. 2020).

Here, we provide a 3D architecture model of the 13q32.1 region that suggests that MCOR-related deletions consistently alter the boundary between two interacting Topologically Associating Domains (TADs). Deleting the critical 35 Kb MCOR-causing region in mice leads to aberrant *Sox21* (MIM*604974) expression in developing and adult iris and CB, aligning precisely with *Dct* (MIM*191275), that is located in the adjacent TAD. This suggests ectopic *Sox21* expression may stem from *Dct* regulatory element adoption, supporting the alteration of TAD boundaries.

Additionally, we identify *Tgfb2* (MIM*190220) as a SOX21 target gene and TGFB2 accumulation in the aqueous humor of a MCOR-affected patient. This accumulation, known for its role in glaucoma and potential impact on axial myopia, underscores the significance of SOX21-TGFB2 signaling in these ocular anomalies and iris development. Insights from congenital microcoria studies may offer therapeutic avenues for individuals with this condition, as well as those with primary open-angle glaucoma (POAG) and high myopia, affecting millions.

RESULTS

MCOR-causing deletions are predicted to alter the boundary between two neighbor topologically associated domains on chromosome 13q32.1

The MCOR locus, defined by its most distant deletion boundaries, spans 99.8 Kb pairs on chromosome 13q32.1 (chr13: 95 209 609 - 95 309 380; Angée et al. 2021). According to Hi-C sequencing data available on the 3D Genome Browser, this locus was originally situated within a one megabase (Mb) TAD, encompassing the genomic region extending from *DCT* (MIM*191275) to *UGGT2* (MIM*605898) genes. Utilizing higher-resolution Hi-C sequencing data obtained from mouse neural progenitor cells, we refined the structural organization of the 13q32.1 region through the detection of two interacting TADs of 1.2 (TAD1) and 1.5 Mb

(TAD2), respectively (**Figure 1A, B**). TAD2 that comprises the original 1 Mb TAD can be broken down into three interacting sub-TADs of 0.2 (TAD2.1), 0.5 (TAD2.2), and 0.2 (TAD2.3) Mb, respectively. Remarkably, all documented deletions associated with MCOR, as reported by Angée et al. in 2021, exhibit modifications at the interface between TAD2.1 and TAD2.2, along with alterations within the regions of both TADs that engage in mutual interactions (**Figure 1A, 1B**). This underscores the significance of the boundary between TAD2.1 and TAD2.2 and emphasizes the intricate interplay within these topologically associating domains in the context of MCOR. None of the reported deletions have an impact on TAD1 or subTAD2.3 (**Figure 1A, 1B**).

The human MCOR locus at 13q32.1 aligns with a broad syntenic region on mouse 14qE4, covering TADs 1 and 2

Through a comparison of human and mouse genomic sequences, we demonstrate that TADs 1 and 2 reside within a large block of synteny shared by human chromosome 13q32.1 and mouse chromosome 14qE4, with minimal changes in gene composition and organizational structure occurring outside the subTADs 2.1 and 2.2 (**Figure 1C, 1D**). Based on the observed synteny, we generated C57BL/6 transgenic mice (B6.cΔMCOR) by using the CRISPR-Cas9 methodology to specifically delete the critical MCOR sequence. This approach was undertaken to investigate its regulatory architecture and to gain insights into its role in iris development, as well as its potential connections to glaucoma and high myopia.

Homozygosity for the critical MCOR causing deletion is lethal in C57BL/6 mice

Mating of heterozygous B6.cΔMCOR/+ failed to produce homozygous B6.cΔMCOR/cΔMCOR animals. Collected of embryos from 8.5 to 10.5 embryonic days (E) showed that homozygous animals ceased developing around E8.5 and regressed by E9.5 (not shown). Further analysis of E9 embryos revealed that homozygous mutants displayed noticeable abnormalities, including smaller size, varying degrees of cardiac hypertrophy, and one individual exhibited pericardial effusion consistent with compromised cardiac function. Additional anomalies included hypoplastic optic and otic vesicles, enlargements in specific facial structures, and irregularities along the body axis (**Figure S1A**).

For in-depth analysis of these abnormalities in homozygous embryos, serial histological sections were conducted (**Figure S1B**). Mutant embryos exhibited pyknotic nuclei in key

regions, including the neural tube, hindbrain, and neural crest-derived tissues such as branchial arches and spinal primordia. Massive pyknosis was observed in these neural crest-derived tissues. Additionally, scattered pyknotic cells were found in mesenchyme, neural tube, and endodermal regions throughout the embryos (**Figure S1B)**. Although the mutant embryos displayed a well-regionalized and differentiated heart, the presence of red blood cells was noticed in the pericardium, potentially indicating myocardium issues. While the myocardium in mutants was thinner compared to controls, their developmental delay complicated conclusive assessments of abnormal differentiation (**Figure S1B)**. Of note, placenta sections showed no apparent differences between mutants and controls (not shown), suggesting that observed cardiovascular abnormalities are not linked to placental defects.

Together these observations, in particular the pattern of pyknosis in mutant embryos, support defective neural crest migration and differentiation.

Heterozygosity for the critical MCOR causing deletion causes reduced pupil size

In contrast to homozygous animals, heterozygous littermates (B6.cΔMCOR/+; referred to thereafter as the MCOR-mouse model) developed normally (**Figure S1A**). Pupillometry analysis in adult animals revealed a moderate but statistically significant ($p<0.01$) reduction in base-line pupil size compared to B6.WT (Wild-Type) littermates (**Figure 2**). Exposure to mydriatic drugs enabled pupil dilation in both B6.cΔMCOR/+ and B6.WT animals **(Figure 2**). B6.cΔMCOR/+ irises were not transilluminable.

***Sox21* in TAD2.2 and its product are ectopically expressed in iris tissue of the MCOR mouse model**

To examine the impact of the critical MCOR-causing deletion on gene expression in iris tissue, we performed transcriptome sequencing on newborn B6.cΔMCOR/+ and B6.WT irises. Consistent with heterozygosity for the deletion which alters *Tgds* (MIM*616146) and *Gpr180* (MIM*607787), the mRNA levels of these two genes in B6.cΔMCOR/+ animals were approximately half of those found in B6.WT specimens (0.49 and 0.60, respectively; $p < 10e-4$).

Further analysis of the genes localized in the three predicted interacting subTAD within TAD2 revealed *Sox21* expression in irises from B6.cΔMCOR/+, while no expression was

observed in B6.WT littermates ($p < 10e-9$). This observation strongly suggests that the critical MCOR-causing deletion induces ectopic expression of *Sox21*, a gene encoding a transcription factor belonging to the SRY-related HMG-box family located in subTAD2.2, approximately 50 kb downstream of the 3'MCOR locus boundary (**Figure 1**). The expression of the other genes located in the interacting TADs displayed comparable expression in mutant and WT irises (not shown).

RT-qPCR and Western blot analyses were conducted on iris RNA and protein extracts from adult mice using specific primers for *Sox21* and a highly specific SOX21 antibody (Matsuda et al. 2012), respectively. These analyses confirmed the sustained ectopic expression of *Sox21* in adulthood (**Figure 3A**) and disclosed the presence of a protein product in B6.cΔMCOR/+ mice, conspicuously absent in B6.WT littermates (**Figure 3B and C**).

Sox21 is detected specifically in DCT-expressing cells from the iris and ciliary body of the MCOR-mouse model

Immunohistochemistry (IHC) analysis of the iris in C57BL/6 animals is challenging due to the high pigmentation of the tissue. To circumvent potential alterations to iris integrity caused by depigmentation protocols, we opted to generate albino cΔMCOR/+ and WT lines by mating B6.cΔMCOR/+ animals with tyrosinase (TYR, MIM*606933)-negative Swiss albino (CFW) mice. RT-qPCR analysis of *Sox21* expression in irises of 2-month-old animals from the resulting lines, referred to as SW.cΔMCOR/+ and SW.WT, revealed continued ectopic expression, despite the inactivation of tyrosinase (data not shown). We performed IHC analysis on iris and CB sections from adult animals using antibodies specific to SOX21 and DCT antibodies, respectively. DCT, also recognized as TYRP2, encodes the dopachrome tautomerase and operates as a melanogenic enzyme located just downstream of tyrosinase. It serves as a distinctive marker for melanocyte lineages, encompassing the pigmented epithelium layers of the iris and CB, respectively the iris posterior and CB anterior layers. *Dct* gene is positioned in TAD2.1 and a mere 75 Kb upstream of the 3'-boundary of the MCOR locus (**Figure 1A and B**). IHC exhibited robust staining of DCT in both the iris posterior and CB anterior epithelia in both SW.cΔMCOR/+ and SW.WT animals (**Figure 3C**). This observation indicates that neither the deletion of the critical MCOR region nor the inactivation of tyrosinase has any discernible effect on the expression of the *Dct* gene in albino mice. Interestingly, in SW.cΔMCOR/+ animals, *Sox21* expression was limited to *Dct*-expressing epithelium layers of

the iris and CB (**Figure 3C**). At this age, we observed no SOX21 staining in the anterior layer of the iris, which is the region from which the dilator muscle forms during the embryonic life (**Figures 3C**). Consistent with the ectopic expression of *Sox21* in mutant mice, SOX21 was undetectable in the iris and CB of SW.WT littermates (**Figure 3C**).

Combining RNAscope™ *In Situ* Hybridization (ISH) of *Sox21* mRNA and immune staining of DCT, we investigated their spatio-temporal pattern of expression from 10 embryonic days (E) to birth (postnatal day 0, P0) in SW.WT and SW.cΔMCOR/+ eyes (**Figure 4**). In WT eyes, *Sox21* mRNA was detected in the proximal part of the optic vesicle (OV) at E10 and in the dorsal neuroectoderm at E10.5 and E11. However, from E11.5 onwards, although the DCT protein became evident, *Sox21* mRNA was no longer detectable, except in the surface ectoderm forming the eyelid and hair follicles, beginning around E15 (**Figure S2**). In mutant eyes, *Sox21* mRNA was initially detectable in the proximal part of the OV at E10 and in the dorsal neuroectoderm at E10.5 and E11, similar to its expression in WT littermates. However, from E10.5 onwards, *Sox21* mRNA was observed in the outer layer of the optic cup (OC) and later in the pigmented structures derived from this layer (**Figure 4A**). Notably, these pigmented structures in the developing eye include the retinal pigmented epithelium (RPE), as well as the iris anterior (reversed in adults) and CB anterior epithelia (**Figure 4B**). Notably, these structures consistently expressed the DCT protein, which became readily detectable from E11.5 onward (**Figure 4A and B**).

The absence of *Sox21* expression in the non-pigmented posterior epithelium layer of both the developing and adult CB, along with the loss of both *Sox21* and DCT expression in the adult anterior epithelium of irises compared to developing irises (Figures 3D and 4), further strengthens the evidence for the co-expression of *Sox21* and DCT in SW.cΔMCOR/+ eyes (**Figure 4A and B**).

Combined analysis of SOX21 targets and gene expression deregulation suggests perturbations in genes associated with iris development and MCOR-related symptoms in the MCOR-mouse model

We investigated the impact of the loss of the critical MCOR-causing region on the expression of genes lying outside of TADs 1 and 2 by analyzing RNAseq data from the new-born B6.cΔMCOR/+ and B6.WT. This study detected 2500 differentially expressed genes (DEG ≥ 1.5 fold change (FC), $p<0.05$; **Figure 5A**). Gene Ontology (GO) enrichment analysis

revealed a significant enrichment of genes associated with crucial processes such as cellular commitment, development, differentiation, and migration, particularly in the context of neural and sensory systems. Notably, the top pathways identified include cell fate commitment, forebrain development, regulation of cell differentiation, retina morphogenesis, regulation of neuron differentiation, and neuron projection development (**Figure 5B**). Consistent with these findings, previous research has highlighted the role of SOX21 in regulating adult neurogenesis *in vivo*, contributing to the generation of new neurons by repressing *Hes5* expression (Matsuda 2012). Notably, our study reveals a downregulation of *Hes5* in the B6.cΔMCOR/+ irises (FC = 0.56, $p < 0.01$), aligning with the established regulatory function of SOX21. Moreover, our study identified additional genes associated with neurogenesis that display altered expression and direct interaction with SOX21. Specifically, we observed significant changes in the expression levels of *SOX2* (MIM* 184429; FC = -1.85, $p < 0.01$), *SOX5* (MIM* 604975; FC = 1.55, $p < 0.01$), *SOX6* (MIM* 60725; FC = 2.02, $p < 0.01$), *DSCAML1* (MIM* 611782; FC = -3.15, $p < 0.01$), and *DTX1* (MIM* 602582; FC = 1.59, $p < 0.01$) (**Figure S3**).

Interestingly, SOX2 plays a critical role in eye development, contributing significantly to the differentiation process during the formation of the anterior segment of the eyes. Numerous studies have reported on the interaction between SOX21 and SOX2, demonstrating a synergistic or antagonistic effect of SOX2 and SOX21 when co-expressed, contingent upon the specific tissue or environmental stimuli (Mallanna et al. 2010; Freeman and Daudet, 2012; Whittington et al. 2015; Goolam et al., 2016). Notably, SOX21 has been identified as an inhibitor of *Sox2* expression in chickens (Freeman and Daudet, 2012), and it has been shown to exert a negative regulatory influence on *SOX2* in human glioma cells (Ferletta et al. 2011). In accordance with these established associations, our study observed a downregulation of *Sox2* in the irises of B6.cΔMCOR/+ mice when compared to their B6.WT counterparts (**Figure S3**). This finding aligns with the reported regulatory dynamics between SOX21 and SOX2, highlighting the complexity of their interplay in the context of eye development and suggesting potential implications for the molecular mechanisms underlying anterior segment differentiation.

We have also observed the upregulation of crucial genes associated with major signaling pathways related to iris development. In particular, Wnt/β-catenin, Transforming Growth Factor Beta (TGF-β) and Bone Morphogenetic Proteins (BMPs) signaling pathways. Regarding Wnt/β-catenin pathway, our findings suggest an impact of the critical MCOR deletion on *Wtn2b* (MIM*601968; FC= 3.57, $p < 0.01$), a gene known to play an essential role in specifying iris

progenitor cells toward a myoepithelial fate, thus contributing to the symptoms of MCOR disease. During the initial phases of eye development in both chicken and mouse embryos, the expression of *Wnt2b* is localized to the marginal tip of the developing retina. This specific region gives rise to the pigmented epithelium of the iris. Intriguingly, our observations indicate that *Wnt2b* expression is notably elevated in the dorsal part of this region, precisely where ectopic expression of *Sox21* was detected in the B6.cΔMCOR/+ mice (see **Figure S4A**). This spatial correlation suggests a potential connection between *Sox21* expression and the regional modulation of *Wnt2b*, offering insights into the regulatory mechanisms governing early eye development and the formation of the iris pigmented epithelium.

Considering the others two signaling pathway, BMPs and TGF-β, we observed upregulation in *Bmp7* (MIM*112267; 1.92, $p<0.05$) playing a role in iris smooth muscle generation (Davis-Silberman and Ashery-Padan 2008) and *Tgfb2* (MIM*190220; 1.6, $p<0.01$) known to be involved in the specification of iris and ciliary as well as in GLC (Prendes et al. 2013) and possibly high myopia (Jia et al. 2017) (**Figure S4B**).

An enrichment of genes related to the regulation of smooth muscle cell proliferation was also noted, albeit with a lower significance ranking (top 45; **Figure 5B**). The impact of the critical MCOR-causing deletion on the gene *Des* (MIM*125660), encoding desmin (DES) intermediate filaments, reported to be deficient in the iris anterior epithelium layer of MCOR-affected patients (Simpson and Parsons 1989). This analysis showed reduced expression of the gene in the iris of B6.cΔMCOR/+ compared to B6.WT littermates (0.49, $p = 0.012$).

To investigate whether the diminished pupil size in B6.cΔMCOR/+ could be associated with a reduction in DES abundance, we conducted immunohistochemistry (IHC) on mouse iris sections using antibodies against DES and smooth muscle actin (SMA; not deregulated in RNAseq datasets) as control. While SMA stained both the sphincter and dilator muscle fibers (**Figure S2**), the available DES antibodies proved unsuccessful in detecting the protein in both B6.cΔMCOR/+ and B6.WT irises.

Tgfb2 is a direct target of SOX21 in the iris of the MCOR-mouse model

To determine which of the deregulated genes were targets of SOX21, we conducted ChIP-seq analysis using the SOX21 antibody on irises from newborn B6.cΔMCOR/+ mice. This analysis revealed 25 DNA regions throughout the genome ($p \leq 0.1$), including 10 intragenic (all intronic) and 14 intergenic and 1 in promoter-TSS regions, respectively (**Table**

1). We conducted a search for deregulated (≥ 1.5 fold; $p \leq 0.05$) expression among these genes and nearest genes in cases where the binding occurred outside a gene, in RNA-seq datasets from B6.cΔMCOR/+ compared to B6.WT animals. This analysis identified a unique gene: *Tgfb2* (**Table 1**). The remaining genes either exhibited no expression or showed no deregulation in the iris of both B6.cΔMCOR/+ and B6.WT animals. Binding of SOX21 to *Tgfb2* as determined by ChIPseq was unambiguous ($p<0.0001$) and strongly supported by JASPAR analysis, which searches for a consensus SOX21-binding sequence in the 252 bp intronic region identified by ChIPseq (chr1:186,698,304-186,698,555; GRCm38/mm10 Assembly; 5.9 Kb downstream from the consensus donor splice-site of the 16 kb-long intron 1; **Figure 5A**). This sequence is conserved in the human *TGFB2* intron 1 orthologous region, which comprises many potential transcription factor-binding sites (GRCh38; chr1:218,352,441-218,352,576; **Figure 5B**).

In line with the association between SOX21 and *Tgfb2*, RNAseq analysis revealed dysregulation of the TGFB2 signaling pathway in the iris of B6.cΔMCOR/+ compared to B6.WT littermates (**Figure 5C**).

TGFB2 concentration is elevated in the AH of MCOR patient

The ectopic expression of *Sox21* in the ciliary body (CB), along with SOX21 binding to a regulatory region of the *Tgfb2* and its upregulation in B6.cΔMCOR/+ irises, prompted us to measure TGFB2 concentration in the aqueous humor (AH) of 12-month-old B6.cΔMCOR/+ and B6.WT mice using an ELISA assay. Concentrations, measured from pooled AH from both eyes, exhibited high variability in both WT and mutant eyes. Analysis of a large number of samples revealed no statistical difference between the two groups (**Figure S5**).

However, when analyzing AH samples collected on the same day during cataract surgery in a 45-year-old non-glaucomatous adult MCOR individual from a large French pedigree (Rouillac et al. 1998), as well as in eleven non-MCOR and non-glaucomatous individuals, we observed a significant increase in TGFB2 levels in the patient's AH compared to the controls (**Figure 6**). Notably, the TGFB2 concentration was elevated as well in AH sample collected during cataract surgery in the fellow eye of the MCOR individual, which occurred two weeks after the first eye surgery. This observation provides additional support for the connection between SOX21 and TGFB2, emphasizing the role of TGFB2 in MCOR.

DISCUSSION

Various anatomical analyses have been conducted on post-mortem eyes and iris specimens obtained during ocular surgery from adult individuals affected by congenital microcoria. These analyses revealed significant iris thinning, stromal atrophy, and a deficiency or absence of stromal contractile processes in the anterior iris epithelium, suggesting that the constitutive closure of the iris is linked to a defective development of the iris musculature. However, the mechanisms involved remain elusive, as does the reason why the disease is often associated with an abnormally long eye and high intraocular pressure (reviewed in Angée et al. 2021). We leveraged the recent identification of the genetic etiology of the disease and the accessibility of CRISPR-Cas9 technology to develop a mouse model of the disease, analysis of which provides support for the central role of the SOX21 transcription factor in the pathology.

The role of SOX21 in eye development was documented in the chick and zebrafish (Uchikawa et al. 1999; Lan et al. 2011) but not in the mouse. In the chick, *Sox21* has been reported to be transiently activated during the early phases of optic vesicle morphogenesis and specification in the lens and retina but is no longer expressed afterward (Lan et al. 2011); *Sox21* expression in the eye ceases before the onset of iris development. Loss of Sox21 function in the chick, akin to findings in zebrafish, disrupts normal lens development (Pauls et al. 2012). In contrast, a *Sox21*-knockout mouse model has been reported (Kiso et al. 2009), which exhibited no ocular defects. This finding is consistent with our immunohistological analysis, which detected no expression of *Sox21* in the anterior segment of the developing mouse eye. In our study, we demonstrate that the deletion of the syntenic critical region in the mouse genome, responsible for congenital microcoria in humans, leads to a constitutive expression of *Sox21*. Remarkably, we observed colocalization of *Sox21* and the melanogenic marker DCT in both developing and adult eyes. This observation aligns with the predicted 3D structural organization of the region encompassing the MCOR locus, which situates *Dct* and *Sox21* in two adjacent neighbor TADs, the integrity of which is potentially disrupted by MCOR-causing deletions. Importantly, the genes themselves remain unaltered by any of the MCOR-causing deletions. Disruptions in TADS was shown to influence regulatory mechanisms during organogenesis, potentially leading to developmental defects (Lupiáñez et al. 2015). Within this framework, the loss of boundary between the two TADs in MCOR could instigate a comprehensive reorganization of the region and render *Dct* active enhancers available for *Sox21* expression. In this context, it is crucial to note that enhancer priming has been shown to precede the initiation of gene transcription (Panigrahi and O'Malley 2021; Reddington et al. 2020; Ghavi-Helm et al.

2014). This, coupled with the fact that our analysis focused on expression of the DCT protein rather than mRNA expression in irises from the mutant mouse, might account for the slight discrepancy observed in our experiments between the detection of *Sox21* mRNA (E10.5) and the detection of DCT protein (E11.5).

Consistent with the expression pattern of the melanogenic DCT protein, the ectopic expression of *Sox21* is detected in the pigmented posterior iris epithelium at the adult age in the MCOR-mouse model, while it is absent in the anterior epithelium responsible for dilator muscle formation (Lai 1972; Forrester et al. 2016). During embryonic development, however, the anterior iris epithelium is pigmented and expresses DCT. The literature lacks reports on the development of iris muscles in mice, but in rats, the dilator muscle begins development around E18.5 and continues postnatally (Lai 1972). In our study, at E18.5 and P0 in mice, we found that the anterior iris epithelium expresses DCT in the WT mouse and both DCT and *Sox21* in the MCOR-mouse model. This suggests that the abnormal expression of Sox21 in the anterior epithelium of the MCOR-mouse model coincides with the onset of dilator muscle development and diminishes progressively during postnatal development, concurrent with the loss of DCT expression in the anterior epithelium (**Figure 4**). These findings could explain histological observations of microcoric irises, revealing anomalies ranging from poor differentiation and disordered fibers lacking myofilaments and intermediate filaments to complete growth inhibition, which point to anomalies in the terminal differentiation stages of anterior iris pigment epithelium (Reviewed in Angée et al. 2021). In the mouse, our histological analysis failed to detect such anomalies. This could be attributed to the minimal iris phenotype of the mutant mouse, potentially linked to weaker *Sox21* expression, divergent timelines in iris dilator muscle development, or dissimilarities in the 3D architecture of the region encompassing the MCOR locus between humans and mice. While the iris phenotype in the mutant mouse is minimal, it is noteworthy that we observed a reduced expression of desmin in the iris of newborn mutant mice. This finding aligns with studies on iris anatomy, which report the absence or severe reduction of desmin fibers in the anterior epithelium of microcoric irises (as reviewed in Angée et al. 2021).

The reduced expression of desmin was identified through RNAseq analysis, given the absence of suitable antibodies for immunocytochemistry analysis. Furthermore, RNAseq analysis revealed the deregulation of key genes known to be crucial in signaling pathways important for iris development. Notably, *Wnt2B*, a gene with significant roles in iris specification and morphogenesis (as reviewed in Noa Davis-Silberman and Ruth Ashery-

Padan, Brain Research, 2008), was found to be significantly upregulated in mutant irises. This deregulation appears to be indirect to *Sox21* induction, as indicated by ChIPseq analysis which did not reveal binding of the SOX21 protein on *Wnt2b* regulatory sequences. Among the deregulated genes identified by RNAseq, *Tgfb2* is the sole gene found to bind SOX21 in mutant irises. This binding occurs through a consensus binding sequence located in intron 1. This observation aligns with a growing body of evidence across various organisms, suggesting that for a subset of genes, the critical sequences regulating expression are not primarily situated in the promoter but within introns within the first kilobase of transcribed sequences (Rose 2019).

Presently, the specific mechanisms responsible for the observed default in muscle development, observed in both the mouse model and individuals affected by MCOR, remain elusive. One plausible hypothesis suggests the involvement of TGFB2. This factor is notably secreted within the periocular mesenchyme and plays a pivotal role in the development of various ocular components, including the anterior chamber—critical for aqueous humor outflow—and the stroma of the iris and ciliary body (Ittner et al. 2005). Although the iris dilator muscle originating from the optic cup margin, derived from neuroectoderm, its myofibers manifest within the stroma. Therefore, an aberrant expression of *TGFB2* within the iris could potentially disrupt stromal development, subsequently affecting the proper formation of the dilator muscle within this context. This proposed link underscores the importance of investigating the interplay between TGFB2 signalling and muscle development in the iris, offering a potential avenue for understanding the muscle-related anomalies observed in the context of MCOR.Remarkably, several studies reported significantly elevated levels of TGFB2 in the aqueous humor of individuals with primary open-angle glaucoma (POAG), as well as in cultured glaucomatous cell strains and isolated human glaucomatous trabecular meshwork (TM) tissues (Wordinger et al. 2014; Agarwal et al. 2015). The cause and cellular source of TGFB2 in glaucomatous eyes remain elusive. However, studies have demonstrated that cells from the trabecular meshwork, through which aqueous humor is drained out at the iridocorneal angle, express an active TGF receptor complex and respond to exogenous TGFB2 (Medina-Ortiz et al. 2013; Montecchi-Palmer et al. 2017). This has been reported to result in increased synthesis of extracellular matrix proteins (ECM), accumulation of which increases resistance to aqueous outflow, leading to elevated intraocular pressure and glaucoma in both human and mouse (Zeimer et al. 1998; Munemasa and Kitaoka 2012; Prendes et al. 2013; Oikawa et al. 2023).

This knowledge, combined with (i) the histopathologic examination of trabecular meshwork (TM) biopsies from two microcoric brothers with elevated IOP, that revealed ECM accumulation (Tawara et al. 2005), and (ii) an elevated concentration of TGFB2 in the aqueous humor of an individual with MCOR, implies that glaucoma associated with MCOR may be initiated by SOX21. The strength of this inference is heightened by our findings, which provide evidence of ectopic *Sox21* expression in the ciliary body—where the aqueous humor is produced—specifically in the non-pigmented posterior epithelium (Skalicky 2016). Furthermore, a recent study has uncovered a significant correlation between elevated TGFB2 levels in the aqueous humor and axial elongation. This discovery not only suggests a connection between the protein and, by extension, SOX21 but also extends the potential link to high myopia (Jia et al. 2017).

Finally, we demonstrate that homozygosity for the critical MCOR-causing deletion is lethal in the mouse. While the possibility of *Sox21* playing a role cannot be ruled out, it is more likely that lethality results from the homozygous deletion of *Tgds*. Notably, biallelic mutations in *TGDS* have been documented to lead to a severe developmental disorder characterized by the Pierre Robin anomaly, known as Catel-Manzke syndrome (MIM# 616145). Intriguingly, to our knowledge, no instances of homozygosity or compound heterozygosity for loss-of-function alleles was reported, suggesting that such a situation could be lethal.

In conclusion, our study demonstrates that the critical submicroscopic deletion associated with MCOR potentially disrupts the 3D architecture of the region, leading to modified gene interactions. This alteration results in the ectopic expression of the Sox21 transcription factor in Dct-expressing pigmented cells within the iris and ciliary body of MCOR mice. Importantly, we posit that in MCOR, both GLC and high myopia stem directly from SOX21-mediated TGFB2 overexpression in the ciliary body, rather than arising due to abnormal iris development. Consequently, we propose that SOX21 serves as a crucial link, connecting iris malformation, high myopia, and glaucoma in congenital microcoria. This positions MCOR as an invaluable model for scrutinizing eye development and unraveling the underlying mechanisms of common myopia and primary open-angle glaucoma.

MATERIALS AND METHODS

Generation of a MCOR-mouse model

The B6.cΔMCOR strain utilized in this study was generated through CRISPR/Cas9 methodology at the Transgenesis Platform of the Animal Facility (LEAT) at the Imagine Institute (Paris). Animal procedures received approval from the French Ministry of Research and were conducted in compliance with the French Animal Care and Use Committee from the University of Paris Cité (APAFIS #14311-201801151627355). Two guide RNAs (sgRNAs, 5'-CTCACAGTTTGGTCCAGGCT-3' and 5'-ATTCCCCAGCAGAGAGGCGC-3') targeting the MCOR locus were designed using the CRISPOR web tool (http://crispor.tefor.net/). Deleterious alleles were induced via CRISPR/Cas9 ribonucleoprotein (RNP) complex microinjection into C57BL/6 mouse zygote pronuclei, as described by Ucuncu in 2020. Offspring were genotyped from genomic DNA through PCR amplification using appropriate primers (forward 5'-GGATGTGCGTTCAAATCCCAGTACC-3' and reverse 5'-TGTTCCCATGCAGTGTGGCAATG-3'). To eliminate potential off-target mutations, transgenic animals underwent multiple generations of backcrossing with C57BL/6 mice. SW.cΔMCOR/+ animals were obtained by crossing B6.cΔMCOR/+ with Swiss albino mice over several generations.

Pupillometry analysis

Two-month-old mice (8 B6.WT and 8 B6.cΔMCOR/+) underwent dark adaptation overnight, and pupillary responses were recorded following established protocols (Kostic et al. 2016). To avoid the potential effects of anesthesia, animals were not anesthetized. The baseline pupil diameter was defined as the mean pupil diameter during the 500 ms before light onset. Subsequently, all pupil sizes were normalized relative to this baseline value. The light stimulus sequence comprised 50 ms exposures to (-2.2, -1, and 0.5) log W/m2 white light and a 20s exposure to 0 log W/m2 blue light. Pupil diameter was automatically determined using Neuroptics A2000, Inc. software. One-way/two-way ANOVA analyses were employed to identify significant differences.

RNA extraction

Mice aged from 0 days postnatal (P0) to 12 months, were euthanized, and their eyes were enucleated. On ice, the eyes were dissected to collect the iris and ciliary body. Each eye was halved following the ora serrata, and after lens removal, the iris and ciliary body were extracted from the anterior segment. Tissues from both eyes were pooled for total RNA extraction using the RNAeasy MiniKit (Qiagen, Hilden, Germany), following the manufacturer's instructions, post-mechanical tissue disruption. RNA quality and concentration were assessed through optical density measurements (Nanodrop, Thermo Fisher Scientific, Waltham, MA, USA), and RNA integrity was analyzed using capillary electrophoresis with a Tape Station (Agilent, Santa Clara, CA, USA) and High Sensitivity RNA Screen Tape.

RNAseq analysis

The Ovation Mouse RNA-Seq System from NuGEN (Tecan Genomics, Leek, NL) was employed to prepare RNA-seq libraries using 25 ng of total RNA, following the manufacturer's recommendations. This kit enables strand-specific RNA-Seq library construction using 10 to 100 ng of total RNA and utilizes the Insert Dependent Adaptor Cleavage (InDA-C) technology to eliminate ribosomal RNA transcripts. An equimolar pool of the final indexed RNA-Seq libraries was sequenced on an Illumina HiSeq 2500, targeting a sequencing depth of approximately 30 million paired-end reads per library. On average, 28 million reads were obtained. FASTQ files were mapped to the ENSEMBL Mouse (MM10) reference using Hisat2 and counted by feature. Counts from the Subread R package. Read count normalizations and group comparisons were conducted using three independent and complementary statistical methods (Deseq2, edgeR, LimmaVoom). Flags were generated from counts normalized to the mean coverage, where counts <20 were considered as background (flag 0) and counts >=20 were considered as signal (flag=1). P50 lists, utilized for statistical analysis, grouped genes showing flag=1 in at least half of the compared samples. Results from the three methods were filtered at p-value <= 0.05 and fold changes of 1.2/1.5/2, and grouped by Venn diagram. Cluster analysis employed hierarchical clustering with the Spearman correlation similarity measure and ward linkage algorithm. Heat maps were generated using the R package ctc: Cluster and Tree Conversion and visualized with Java Treeview software. Functional analyses were conducted using Ingenuity Pathway Analysis (IPA, Qiagen).

RT-qPCR analysis

cDNA was synthesized using the cDNA Verso reverse transcription kit (Thermo Fisher Scientific). Quantitative RT-PCR (RT-qPCR) was conducted using SYBR Green (Sso Advanced Universal SybrGreen Supermix, Bio-Rad, Hercules, CA, USA), with *B2m*, *Tbp*, *Gusb* and *Hprt* as reference genes. The primer sequences for qPCR were as follows: *Sox21* forward 5'-AGCCTGTGGACCACGTCAA-3' and reverse 5'-CCGACTCGGTGAGCAGCTT; *Dct* forward 5'-AGATTGTGTGCGACAGCTTG-3' and reverse 5'-AAGGGAGGGCTGTCAAACTT-3'; *B2m* forward 5'-CCTGTATGCTATCCAGAAAACCCCT-3' and reverse 5'-CGTAGCAGTTCAGTATGTTCGGCTT-3'; *Tbp* forward 5'-TGACCTAAAGACCATTGCACTTCGT-3' and reverse 5'-CTGCAGCAAATCGCTTGGGA-3'; *Gusb* forward 5'-CTGGGGTTGTGATGTGGTCTGT-3' and reverse 5'-TGTGGGTGATCAGCGTCTTAAAGT-3'; *Hprt* forward 5'-GTTGGTACAGGCCAGACTTTGTT-3' and reverse 5'-AAACGTGATTCAAATCCCTGAAGTA-3'. The relative expression of *Sox21* and Dct was calculated using the method described in Vandesompele et al. 2002.

Western blot analysis

The western blots were performed using 40 μg of total iris protein lysates. The following antibodies were used in this study: SOX21 (AF3538, R&D Systems, Minneapolis, MN, USA) and beta-Actin (ab8227, Abcam, Cambridge, UK). Secondary antibodies, goat IgG or mouse IgG HRP (Thermo Fisher Scientific) were used at a 1:10000 dilution. Western blot membranes were developed using the Clarity Western ECL substrate (Bio-Rad), and the signal was detected with a Chemidoc MP Imaging System (Bio-Rad).

ChIPseq analysis

The irises of 24 newborns (P0), including both B6.cΔMCOR/+ and B6.WT mice, were collected for ChIP-seq analysis. Three samples were prepared for B6.cΔMCOR/+ mice and three for B6.WT mice, with each sample comprising 16 irises. The ChIP assay was performed on all samples using 2 μg of chromatin.

Cells were crosslinked with 1% formaldehyde for 10 minutes at room temperature. ChIP was carried out using the iDeal ChIP-seq kit for Transcription Factors (C01010055, Diagenode, Liege, Belgium), following the provided protocol. Immunoprecipitation utilized an anti-SOX21 antibody (AF3538, R&D Systems). Sequencing was performed on an Illumina HiSeq 4000, running HiSeq Control Software HD version 3.4.0.38. Quality control of sequencing reads was conducted using FastQC. Reads were aligned to the reference genome (MM10) from the UCSC genome browser using BWA software v.0.7.5a. All samples were filtered using a list of genomic regions created from the two input samples. Subsequently, samples were deduplicated using SAMtools version 1.3.1. Alignment coordinates were converted to BED format using BEDTools v.2.17, and peak calling was performed using MACS2.

ELISA assay

Mice were euthanized at 5, 6, and 12 months old, and aqueous humor (AH) was collected from both eyes using a 27G-syringe inserted at the ora serrata (around 5 µL per eye). The AH from both eyes was pooled, and TGFB2 proteins from the samples were activated using one volume of HCl and two volumes of NaOH, as per the manufacturer's instructions (Mouse TGF-beta 2 Quantikine ELISA Kit, R&D Systems). The samples were diluted (1:80), and the quantity of total inactive TGFB2 protein was measured using the Quantikine kit.

Human AH was collected from ten patients undergoing cataract surgery at Clinique Jules Verne, Nantes, France. The mean age of the nine controls was 76.7 ± 5 years old, while the MCOR patient was the youngest at 44 years old. All samples were collected with the written and informed consent of the patients. TGFB2 dosage in each eye (13 controls + 2 cases) was conducted with the Human TGF-beta 2 Quantikine ELISA kit (R&D Systems), following the provided instructions.

Immunofluorescence and RNAscope analysis

Pregnant mice were euthanized to collect embryos at various stages, from E10.5 to P0. Accurate embryonic stages were assigned post-cutting by consulting established atlases due to variations in early embryo development within littermates. Embryo heads were fixed with 4% Paraformaldehyde (PFA), and fixed heads as well as fresh adult eyes were embedded in Optimal Cutting Temperature (OCT) compound and frozen in liquid nitrogen for rapid tissue freeze. OCT blocks were stored at -80°C and brought up to -20°C prior to cutting (CM3050S, Leica,

Wetzlar, Germany). Frozen tissue sections (14µm thickness) were collected at the level of the pupillary aperture, air-dried, and stored at -80°C.

Frozen sections were rinsed in PBS to remove surrounding OCT, and antigen retrieval was performed using Citrate Buffer (pH 6.0) in a 95°C water bath for 30 minutes. Slides were then cooled for 30 minutes at room temperature. Tissues were blocked for 1 hour in PBS with 1% bovine serum albumin (BSA), labeled with primary antibodies anti-SOX21 (AF3538, R&D Systems), anti-DCT (ab74073, Abcam), and Cy3-coupled anti-alpha Smooth Muscle Actin (C6198, Sigma-Aldrich, Saint-Louis, MO, USA), followed by appropriate secondary antibodies. Slides were counterstained with DAPI and mounted with Fluoromount medium (Sigma-Aldrich).

For mRNA detection, slides were processed using the RNAscope Multiplex Fluorescent v2 Assay, and subsequent immunohistochemistry was performed. All images were acquired with a Spinning Disk Confocal microscope (Carl Zeiss, Oberkochen, Germany), capturing whole sections with a 10X objective and specific areas of interest (iris, ciliary body, and margins of the optic cup) with a 40X oil-objective. Raw images were converted to TIFF for further analysis using Fiji (v1.53t).

Statistical analysis

Unpaired bilateral Student's t-test was used for two-group analyses. Two-way ANOVA analysis was used for multigroup analyses (GraphPad Prism, ver. 10.0.3). Data are presented as the mean ± SEM; $p<0.05$ was considered significant.

CONFLICT OF INTEREST

The SOX21-TGFB2 pathway in iris development, axial myopia, and glaucoma has been officially patented under the title: "Methods and pharmaceutical compositions for treating ocular diseases" (WO/2021/245224). The inventors of this groundbreaking patent are JMR, LFT, BN, CA, and JK.

ACKNOWLEDGEMENTS

This research has been generously supported by grants from the Agence Nationale de la Recherche (ANR# -20-CE 12-0019-01), the Institut Nationale de la Santé et de la Recherche Médicale (INSERM), MSD Avenir (DEVO-DECODE program), the Fondation Vision, and the Association Retina France.

AUTHOR CONTRIBUTIONS

JMR and LFT designed the project. BP, JLV and PD generated the MCOR mice. CA and EE performed and interpreted the molecular, histological and imaging experiments. DH analyzed the Hi-Cseq data. CK and SC performed the pupillometry experiments. ED, JK, PC, JP and NCh provided clinical data. MZ and CBF performed sequencing of the RNA samples. NCa performed bioinformatic analyses. BN and JC provided technical assistance. CA wrote the manuscript and prepared the figures with contributions from all coauthors. JM and LFT reviewed all of the data and edited the manuscript.

REFERENCES

Agarwal P, Daher AM, Agarwal R. 2015. Aqueous humor TGF-β2 levels in patients with open-angle. *Mol Vis*.

Angée C, Nedelec B, Erjavec E, Rozet J-M, Fares Taie L. 2021. Congenital Microcoria: Clinical Features and Molecular Genetics. *Genes* **12**: 624.

Davis-Silberman N, Ashery-Padan R. 2008. Iris development in vertebrates; genetic and molecular considerations. *Brain Res* **1192**: 17–28.

Fares-Taie L, Gerber S, Tawara A, Ramirez-Miranda A, Douet J-Y, Verdin H, Guilloux A, Zenteno JC, Kondo H, Moisset H, et al. 2015. Submicroscopic Deletions at 13q32.1 Cause Congenital Microcoria. *Am J Hum Genet* **96**: 631–639.

Ferletta M, Caglayan D, Mokvist L, Jiang Y, Kastemar M, Uhrbom L, Westermark B. 2011. Forced expression of Sox21 inhibits Sox2 and induces apoptosis in human glioma cells. *Int J Cancer.* **129**:45-60.

Forrester JV, Dick AD, McMenamin PG, Roberts F, Pearlman E. 2016. Chapter 2 - Embryology and early development of the eye and adnexa. In *The Eye (Fourth Edition)* (eds. J.V. Forrester, A.D. Dick, P.G. McMenamin, F. Roberts, and E. Pearlman), pp. 103-129.e8, W.B. Saunders https://www.sciencedirect.com/science/article/pii/B9780702055546000022 (Accessed September 13, 2023).

Freeman S, Daudet N. 2012. Artificial Induction of Sox21 Regulates Sensory Cell Formation in the Embryonic Chicken Inner Ear. *PLoS ONE*.

Ghavi-Helm Y, Klein FA, Pakozdi T, Ciglar L, Noordermeer D, Huber W, Furlong EEM. 2014. Enhancer loops appear stable during development and are associated with paused polymerase. *Nature* **512**: 96–100.

Goolam M, Scialdone A, Graham SJL, Macaulay IC, Jedrusik A, Hupalowska A, Voet T, Marioni JC, Zernicka-Goetz M. 2016. Heterogeneity in Oct4 and Sox2 Targets Biases Cell Fate in 4-Cell Mouse Embryos. *Cell.* 2016 **165**:61-74.

Gould DB, Smith RS, John SWM. 2004. Anterior segment development relevant to glaucoma. *Int J Dev Biol* **48**: 1015–1029.

Ittner LM, Wurdak H, Schwerdtfeger K, Kunz T, Ille F, Leveen P, Hjalt TA, Suter U, Karlsson S, Hafezi F, Born W, Sommer L. 2005. Compound development eye disorders following inactivation of TGFB signaling in neural-crest stem cells. *Journal of Biology*. **4**:11.

Jia Y, Yue Y, Hu D-N, Chen J-L, Zhou J-B. 2017. Human aqueous humor levels of transforming growth factor-β2: Association with matrix metalloproteinases/tissue inhibitors of matrix metalloproteinases. *Biomed Rep*. http://www.spandidos-publications.com/10.3892/br.2017.1004 (Accessed August 26, 2022).

Kiso M, Tanaka S, Saba R, Matsuda S, Shimizu A, Ohyama M, Okano HJ, Shiroishi T, Okano H, Saga Y. 2009. The disruption of Sox21-mediated hair shaft cuticle differentiation causes cyclic alopecia in mice. *Proc Natl Acad Sci* **106**: 9292–9297.

Kostic C, Crippa SV, Martin C, Kardon RH, Biel M, Arsenijevic Y, Kawasaki A. 2016. Determination of Rod and Cone Influence to the Early and Late Dynamic of the Pupillary Light Response. *Invest Ophthalmol Vis Sci* **57**: 2501–2508.

Lai Y-L. 1972. The development of the dilator muscle in the iris of the albino rat. *Exp Eye Res* **14**: 203–207.

Lan X, Wen L, Li K, Liu X, Luo B, Chen F, Xie D, Kung H. 2011. Comparative analysis of duplicated sox21 genes in zebrafish. *Dev Growth Differ* **53**: 347–356.

Lupiáñez DG, Kraft K, Heinrich V, Krawitz P, Brancati F, Klopocki E, Horn D, Kayserili H, Opitz JM, Laxova R, et al. 2015. Disruptions of topological chromatin domains cause pathogenic rewiring of gene-enhancer interactions. *Cell* **161**: 1012–1025.

Mallanna SK, Ormsbee BD, Iacovino M, Gilmore JM, Cox JL, Kyba M, Washburn MP, Rizzino A. 2010. Proteomic Analysis of Sox2-Associated Proteins During Early Stages of Mouse Embryonic Stem Cell Differentiation Identifies Sox21 as a Novel Regulator of Stem Cell Fate. *Stemm Cell*. **28**: 1715-1727.

Matsuda S, Kuwako K, Okano HJ, Tsutsumi S, Aburatani H, Saga Y, Matsuzaki Y, Akaike A, Sugimoto H, Okano H. 2012. Sox21 Promotes Hippocampal Adult Neurogenesis via the Transcriptional Repression of the Hes5 Gene. *J Neurosci* **32**: 12543–12557.

Medina-Ortiz WE, Belmares R, Neubauer S, Wordinger RJ, Clark AF. 2013. Cellular fibronectin expression in human trabecular meshwork and induction by transforming growth factor-β2. *Invest Ophthalmol Vis Sci* **54**: 6779–6788.

Montecchi-Palmer M, Bermudez JY, Webber HC, Patel GC, Clark AF, Mao W. 2017. TGFβ2 Induces the Formation of Cross-Linked Actin Networks (CLANs) in Human Trabecular Meshwork Cells Through the Smad and Non-Smad Dependent Pathways. *Invest Ophthalmol Vis Sci* **58**: 1288–1295.

Munemasa Y, Kitaoka Y. 2012. Molecular mechanisms of retinal ganglion cell degeneration in glaucoma and future prospects for cell body and axonal protection. *Front Cell Neurosci* **6**: 60.

Oikawa K, Torne O, Sun D, Moon AKB, Kiland JA, Trane RM, McLellan GJ. 2023. Aqueous Humor TGF-β2 and Its Association With Intraocular Pressure in a Naturally Occurring Large Animal Model of Glaucoma. *Invest Ophthalmol Vis Sci* **64**: 18.

Panigrahi A, O'Malley BW. 2021. Mechanisms of enhancer action: the known and the unknown. *Genome Biol* **22**: 108.

Pauls S, Smith SF, Elgar G. 2012. Lens development depends on a pair of highly conserved Sox21 regulatory elements. *Dev Biol* **365**: 310–318.

Pozza E, Verdin H, Deconinck H, Dheedene A, Menten B, De Baere E, Balikova I. 2020. Microcoria due to first duplication of 13q32.1 including the GPR180 gene and maternal mosaicism. *Eur J Med Genet* **63**: 103918.

Prendes MA, Harris A, Wirostko BM, Gerber AL, Siesky B. 2013. The role of transforming growth factor β in glaucoma and the therapeutic implications. *Br J Ophthalmol* **97**: 680–686.

Ramirez-Miranda A, Paulin-Huerta JM, Chavez-Mondragón E, Islas-de la Vega G, Rodriguez-Reyes A. 2011. Ultrabiomicroscopic-histopathologic correlations in individuals with autosomal dominant congenital microcoria: three-generation family report. *Case Rep Ophthalmol* **2**: 160–165.

Reddington JP, Garfield DA, Sigalova OM, Karabacak Calviello A, Marco-Ferreres R, Girardot C, Viales RR, Degner JF, Ohler U, Furlong EEM. 2020. Lineage-Resolved Enhancer and Promoter Usage during a Time Course of Embryogenesis. *Dev Cell* **55**: 648-664.e9.

Rose AB. 2019. Introns as Gene Regulators: A Brick on the Accelerator. *Front Genet* **9**. https://www.frontiersin.org/articles/10.3389/fgene.2018.00672 (Accessed November 11, 2023).

Rouillac C, Roche O, Marchant D, Bachner L, Kobetz A, Toulemont PJ, Orssaud C, Urvoy M, Odent S, Le Marec B, et al. 1998. Mapping of a congenital microcoria locus to 13q31-q32. *Am J Hum Genet* **62**: 1117–1122.

Sergouniotis PI, Ellingford JM, O'Sullivan J, Fenerty CH, Black GC. 2017. Genome sequencing identifies a large deletion at 13q32.1 as the cause of microcoria and childhood-onset glaucoma. *Acta Ophthalmol (Copenh)* **95**: e249–e250.

Simpson WA, Parsons MA. 1989. The ultrastructural pathological features of congenital microcoria. A case report. *Arch Ophthalmol Chic Ill 1960* **107**: 99–102.

Skalicky SE. 2016. The Ciliary Body and Aqueous Fluid Formation and Drainage. In *Ocular and Visual Physiology: Clinical Application* (ed. S.E. Skalicky), pp. 67–83, Springer, Singapore https://doi.org/10.1007/978-981-287-846-5_5 (Accessed August 25, 2023).

Tawara A, Itou K, Kubota T, Harada Y, Tou N, Hirose N. 2005. Congenital microcoria associated with late-onset developmental glaucoma. *J Glaucoma* **14**: 409–413.

Uchikawa M, Kamachi Y, Kondoh H. 1999. Two distinct subgroups of Group B Sox genes for transcriptional activators and repressors: their expression during embryonic organogenesis of the chicken. *Mech Dev* **84**: 103–120.

Ucuncu E, Rajamani K, Wilson MSC, Medina-Cano D, Altin N, David P, Barcia G, Lefort N, Banal C, Vasilache-Dangles M-T, et al. 2020. MINPP1 prevents intracellular accumulation of the chelator inositol hexakisphosphate and is mutated in Pontocerebellar Hypoplasia. *Nat Commun* **11**: 6087.

Vandesompele J, De Preter K, Pattyn F, Poppe B, Van Roy N, De Paepe A, Speleman F. 2002. Accurate normalization of real-time quantitative RT-PCR data by geometric averaging of multiple internal control genes. *Genome Biol* **3**: research0034.1-research0034.11.

Whittington N, Cunningham D, Le TK, De Maria D, Silva EM. 2015. Sox21 regulates the progression of neuronal differentiation in a dose-dependent manner. *Developmental Biology*. **397**: 237-247.

Wordinger R, Sharma T, Clark A. 2014. The Role of TGF-β2 and Bone Morphogenetic Proteins in the Trabecular Meshwork and Glaucoma. *J Ocul Pharmacol Ther Off J Assoc Ocul Pharmacol Ther* **30**.

Zeimer R, Asrani S, Zou S, Quigley H, Jampel H. 1998. Quantitative detection of glaucomatous damage at the posterior pole by retinal thickness mapping. A pilot study. *Ophthalmology* **105**: 224–231.

Gene	Gene Description	Chr	Peak Score	Annotation	Distance to TSS	Nearest PromoterID	RNAseq
Hipk2	Homeodomain interacting protein kinase 2	chr6	104.51 /26.18	intron (NM_010433, intron 2 of 14)	76864	NM_001136065	
Gm13580	Predicted gene 13580	chr2	46.62	Intergenic	-8724	NR_046065	
Gm17644	Predicted gene 17644	chr1	43.95	Intergenic	-22756	NR_045297	
Tgfb2	Transforming growth factor, beta 2	chr1	40.86	intron (NM_009367, intron 1 of 6)	7563	NM_009367	1,6 Up Regulated in HT
Mydgf	Myeloid derived growth factor	chr17	40.64	intron (NM_172624, intron 10 of 20)	-16198	NM_080837	
Olfr854	Olfactory receptor 854	chr9	37.19	Intergenic	-8090	NM_146522	
Tex14	Testis expressed gene 14	chr11	24.63	intron (NM_031386)	-4435	NM_001199293	
Gm4736	Predicted gene 4736	chr6	21.86	Intergenic	-99620	NM_053251	
Slf1	SMC5-SMC6 complex localization factor 1	chr13	20.03	intron (NM_134071, intron 5 of 20)	25853	NM_134071	
4930521E06Rik	RIKEN cDNA 4930521E06 gene	chr1	18.78	Intergenic	-206375	NR_040602	
Ctdsp1	C-terminal domain small phosphatase 1	chr1	17.45	Intergenic	-4548	NM_153088	
Myo7a	Myosin VIIA	chr7	16.1	intron (NM_001256081, intron 39 of 48)	49182	NM_001256083	
AA545190	EST AA545190	chr6	15.75	Intergenic	788031	NR_033776	
Popdc3	Popeye domain containing 3	chr10	15.56	Intergenic	-109987	NM_024286	
Gdnf	Glial cell line derived neurotrophic factor	chr15	14.96	Intergenic	-113169	NM_001301332	
1700128A07Rik	RIKEN cDNA 1700128A07 gene	chr14	14.8	Intergenic	-588884	NR_045938	
Pcdh9	Protocadherin 9	chr14	14.16	Intergenic	1798871	NM_001081377	
Adgrl4	Adhesion G protein-coupled receptor L4	chr3	14.16	Intergenic	-303096	NM_133222	
Nsmce2	Non-SMC element 2 homolog (MMS21)	chr15	14.11	intron (NM_026746)	51552	NM_026746	
Wls	Wntless homolog (Drosophila)	chr3	13.73	intron (NR_037590)	12420	NR_037590	
Nrarp	Notch-regulated ankyrin repeat protein	chr2	12.17	promoter-TSS (NM_025980)	-24	NM_025980	
Cpa6	Carboxypeptidase A6	chr1	11.31	intron (NM_177834)	208422	NM_001289497	
Llph	LLP homolog, long-term synaptic facilitation factor	chr10	11.22	Intergenic	51806	NM_025431	
Cartpt	CART prepropeptide	chr13	10.95	Intergenic	-2410	NM_001081493	
2810404M03Rik	RIKEN cDNA 2810404M03 gene	chr8	10.1	intron (NR_045497)	143286	NR_045497	

Table 1. DNA regions identified by ChIPseq analysis for SOX21 binding in the iris of B6.cΔMCOR/+ mice. The genes listed in this table are restricted to those associated with a Peak score greater than 10, corresponding to a p-value of 0.1 or higher. The peak location is presented relative to the genomic distance from the transcription start site (TSS). Specifically, the 25 sites from the SOX21 ChIP sequencing data were identified in one or more samples, each of which comprised 16 irises.

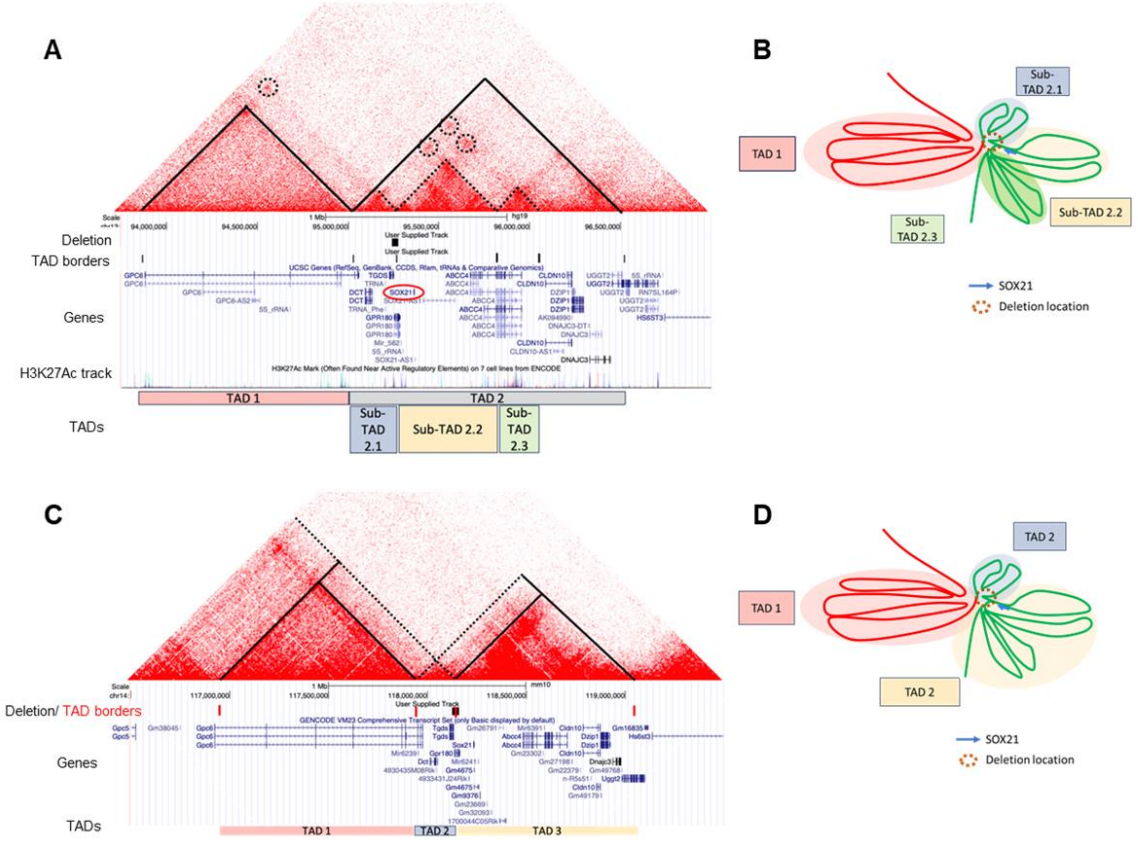

Figure 1: Organization of the MCOR Region in the human and syntenic mouse genomes. A) The 13q32.1 MCOR locus in humans (hg19) is depicted. Based on HiC-seq data from human neural progenitor cells, the region consists of two topologically-associated domains (TADs) spanning 1.2 Megabases (Mb) and 1.5 Mb (in pink and grey, respectively). These TADs are demarcated by black straight lines on the interaction frequency map, with TAD borders indicated in the second track under the interaction map. TAD 2 further reveals at least three discernible sub-TADs: Sub-TAD 2.1 (in blue) covering 0.2 Mb, Sub-TAD 2.2 (in yellow) spanning 0.5 Mb, and Sub-TAD 2.3 (in green) covering 0.2 Mb. Sox21 is located within Sub-TAD 2.2, and the deletion affects the boundary between Sub-TAD 2.1 and Sub-TAD 2.2. Circled dashed lines highlight direct and robust interactions between the deleted region and other regions in various TADs and sub-TADs. **B)** The schematic representation illustrates the chromatin organization at the 13q32.1 locus. TAD 1 and the three Sub-TADs are emphasized in their respective colors. A dashed brown circle line denotes the location of the MCOR deletion, while the blue arrow highlights the Sox21 gene's position in Sub-TAD 2.2. **C)** and **D)** depict the predicted 3D structure of the mouse syntenic region on chromosome 14. This structure closely mirrors the human configuration, demonstrating a high degree of similarity between the two species.

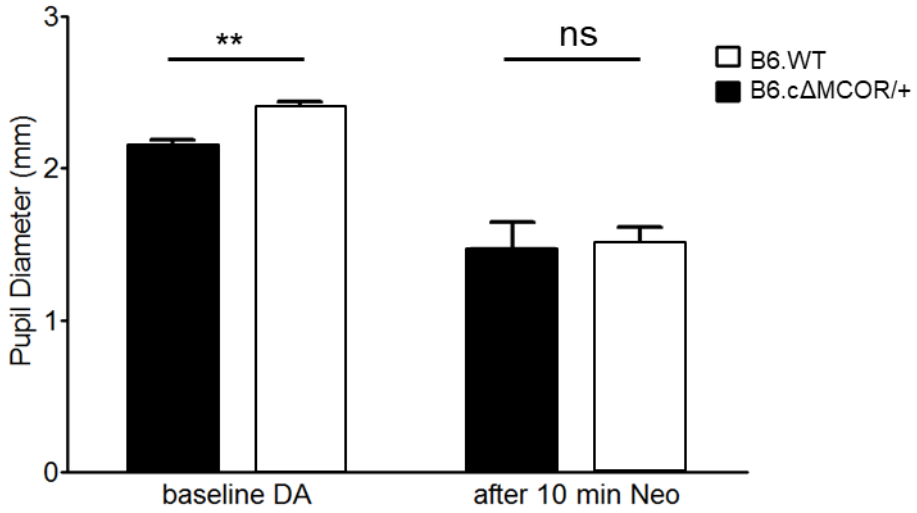

Figure 2: Pupillary Response of cΔMCOR Mice. Pupillometry was employed to assess pupil diameter in B6.cΔMCOR/+ mice, revealing a moderate but statistically significant basal reduction in pupil size compared to B6.WT animals (**: $p<0.01$, $n = 8$ animals per group). Following mydriatic administration (neosynephrin, 10 min), pupil size exhibited no significant difference between the two mouse lines (ns: not significant).

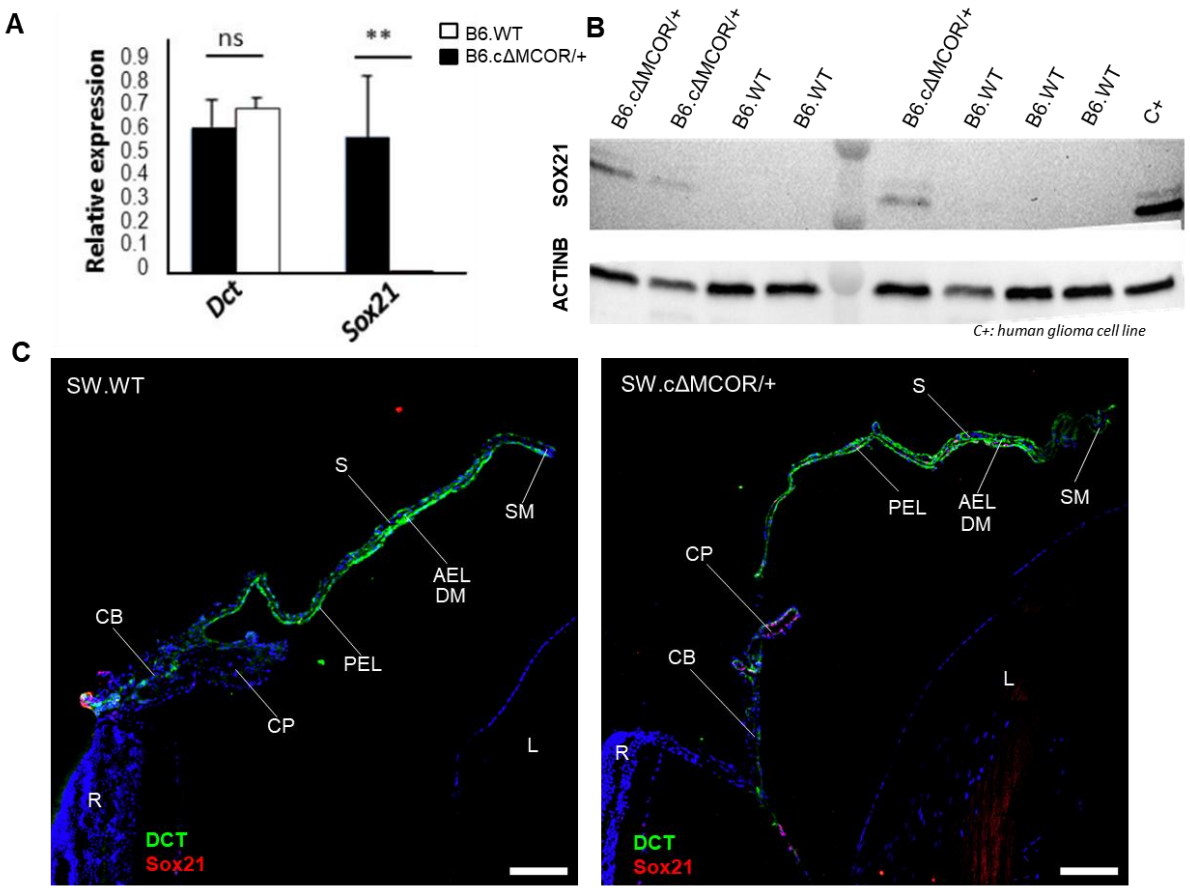

Figure 3: Expression Level Analysis at the 1Mb-TAD, RTqPCR, WB, and HiC Analysis of *Sox21* and its protein product in cΔMCOR and WT Animals. A) RTqPCR analysis of *Dct* and *Sox21* abundance in iris/ciliary body RNA extracts from newborn B6.cΔMCOR/+ and B6.WT mice (n = 5, each group). **B**) Western blot analysis of iris protein extracts reveals the presence of SOX21 in B6.cΔMCOR/+ but not in B6.WT counterparts. ActinB serves as the loading control, and C+ denotes glial cells expressing endogenous SOX21. **C**) Immunohistochemistry (IHC) analysis of iris and ciliary body in newborn B6.cΔMCOR and B6.WT mice, illustrating the detection of SOX21 and DCT in the PEL layer. AEL - iris anterior epithelium layer, **CB**: ciliary body, **CP**: ciliary process, **DM:** dilator muscle, **L:** lens, **PEL:** iris posterior epithelium layer, **R:** retina, **S:** iris stroma, **SM:** sphincter muscle. (Scale bars: 100 µm).

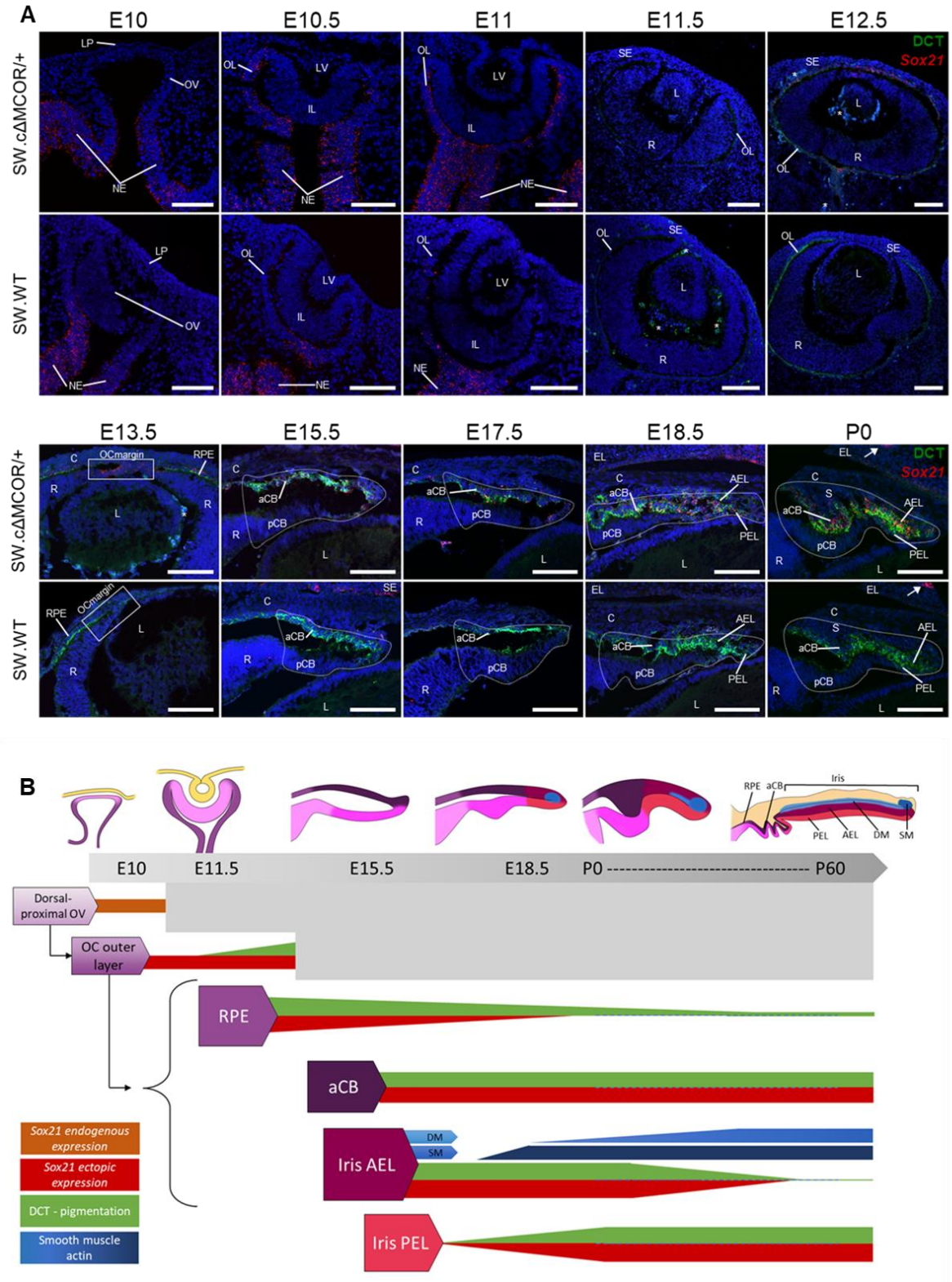

Figure 4. Expression pattern of *Sox21* and DCT during eye development. The spatio-temporal pattern of expression of Sox21 and DCT was assessed using in situ hybridization (ISH) combined with immunofluorescence (IF) on multiple heads at various developmental stages, spanning from the invagination of the optic vesicle into the optic cup to the formation of the iris and ciliary body (**A**). In the images, Sox21 mRNA is stained in red, DCT in green, and autofluorescence, predominantly caused by blood vessels, is visible in cyan (white asterisks).

The overall expression dynamics of Sox21 and DCT during iris development are summarized in the scheme below (**B**). Sox21 is naturally expressed in the proximal region of the developing optic vesicle (OV) (depicted by the orange bar) at embryonic day 10 (E10) and is absent during the subsequent stages of optic cup formation. Around E15.5, endogenous Sox21 is also observed in the eyelid and hair follicles (white arrows). In SW.cΔMCOR/+ animals, Sox21 ectopic expression emerges from E10.5, encompassing the entire outer layer of the optic cup (OC) in red. This layer gives rise to the retinal pigment epithelium (RPE), and the anterior epithelium of both the ciliary body (CB) and iris at its margin (outlined by white dotted lines), around E15.5. Intriguingly, Sox21 misexpression precedes the appearance of DCT (green) in the developing eye. As the RPE differentiates, the reduction in DCT is accompanied by a decline in Sox21 during the late stages of development. The expression of both genes remains stable in the anterior CB epithelium from its development to maturation. Concurrently, the evolution in iris pigmentation aligns with the change in Sox21 expression: the iris anterior epithelium layer (AEL) is initially heavily pigmented (rich in DCT) and loses its melanin, along with Sox21, during postnatal maturation. The posterior epithelium layer (PEL) progressively gains melanin in a centrifugal manner during development, becoming fully pigmented in adulthood, while also expressing Sox21. Notably, the sphincter and dilator muscles (depicted in blue) begin forming around E17.5 and E18.5, respectively, with the dilator maturing long after birth. The shaded box indicates the period from birth to the age of 2 months, during which we currently lack information regarding iris anterior epithelium layer (AEL) pigmentation and the precise stages of dilator muscle (DM) development. **aCB:** anterior ciliary body epithelium, **AEL:** iris anterior epithelium layer, **C:** cornea, **DM:** dilator muscle, **EL:** eyelid, **IL:** optic cup inner layer, **L:** lens, **LP:** lens placode, **LV:** lens vesicle, **NE:** neuroectoderm, **OC:** optic cup, **OL:** optic cup outer layer, **OV:** optic vesicle, **pCB:** posterior ciliary body epithelium, **PEL:** iris posterior epithelium layer, **R:** retina, **RPE:** retinal pigment epithelium, **S:** iris stroma, **SE:** surface ectoderm, **SM:** sphincter muscle. Scale bars: **100µm**.

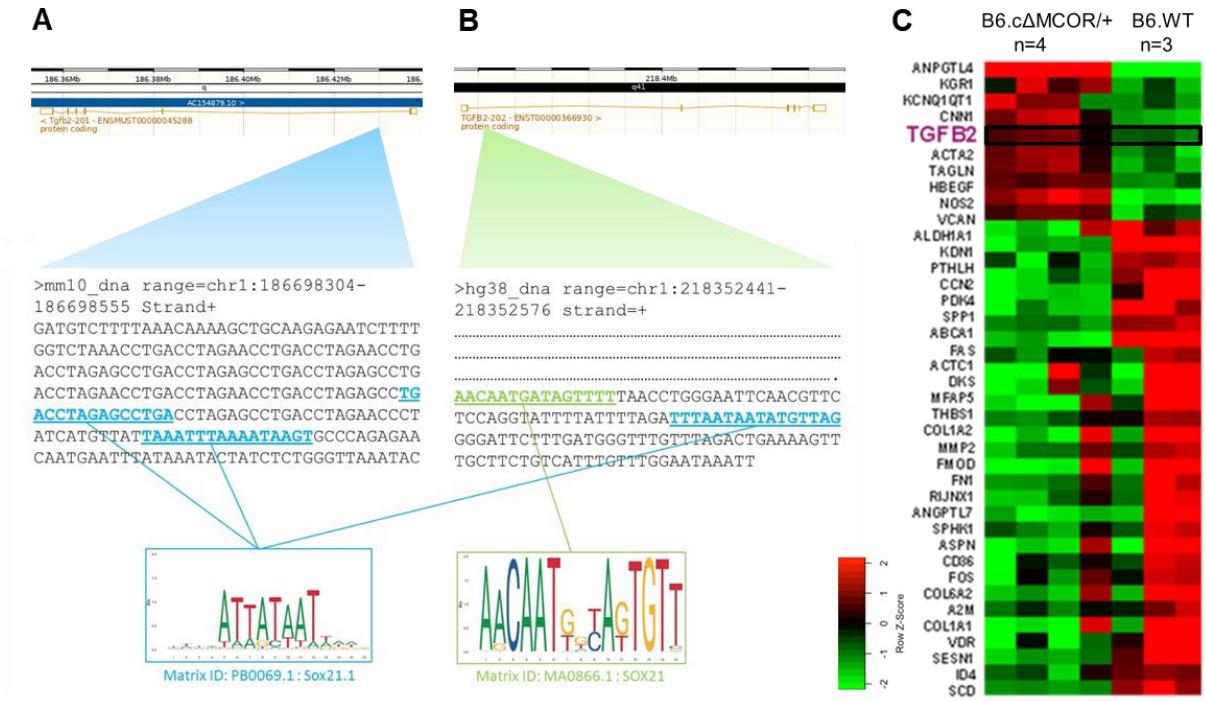

Figure 5. SOX21 consensus binding sequences in mouse and human *TGFB2* gene and RNA-seq analysis of the *Tgfb2* signaling pathway in the B6.cDMCOR/+ mouse as compared to B6.WT counterparts. A) ChIP-seq experiment reveals the DNA sequence binding to SOX21 in the mouse, particularly in the first intron of the *Tgfb2* gene. **B**) The syntenic sequence from the human genome assembly GRCh38, situated in the first intron of the TGFB2 gene, is presented. The SOX21-consensus motif, according to the JASPAR database, is displayed at the bottom of the figure. The mouse binding sequence (PB006.1) of SOX21 is highlighted in blue, found in both the human and mouse sequences in the intron. The human motif (MA0866.1), shown in green, is also present in the *TGFB2* intron 1, suggesting a potential binding of SOX21 in this location. **C**) The RNA-seq heatmap shows genes of the TGFB pathway. While some variations are observable among individuals within the same group, *Tgfb2* is consistently overexpressed in all four cΔMCOR/+ irises.

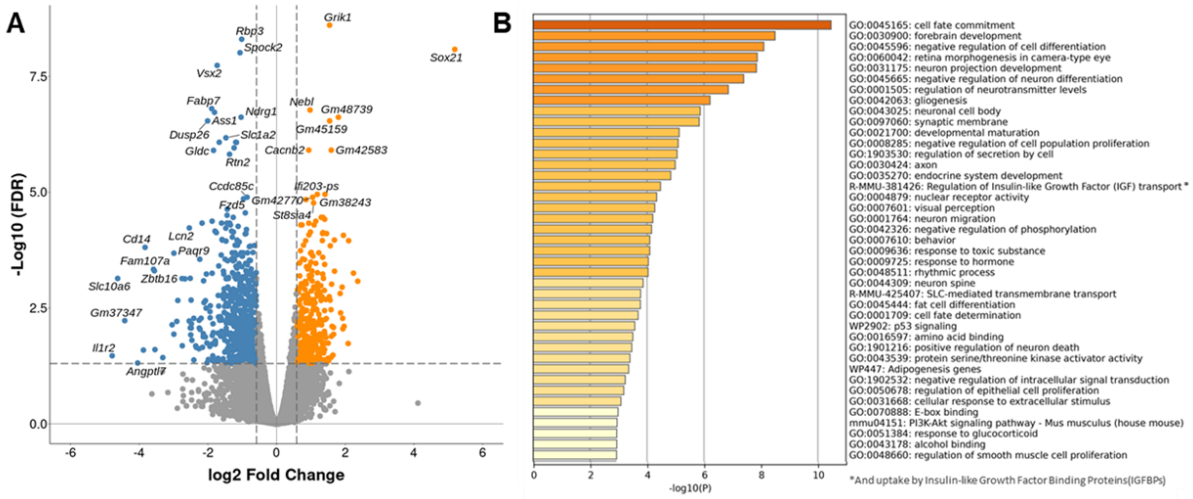

Figure 6. Comparative analysis of gene expression in the iris of B6.cDMCOR/+ versus B6.WT littermates. A) Volcano plots of the most differentially expressed genes (DEGs) from RNAseq data of B6.WT ($N = 3$) and B6.cΔMCOR/+ ($N = 4$) irises at P0. On the x-axis (log2 scale), the difference in gene expression Fold Change (FC) is displayed and False Discovery Rate (FDR) adjusted significance is plotted on the y-axis (log10 scale). Negative values indicate down regulation; positive values indicate up regulation. **B**) Enrichment analysis in the category Biological Processes for most relevant DEGs using Metascape. The input DEGs lists are shown in a heatmap with enriched terms, which are colored by p-values.

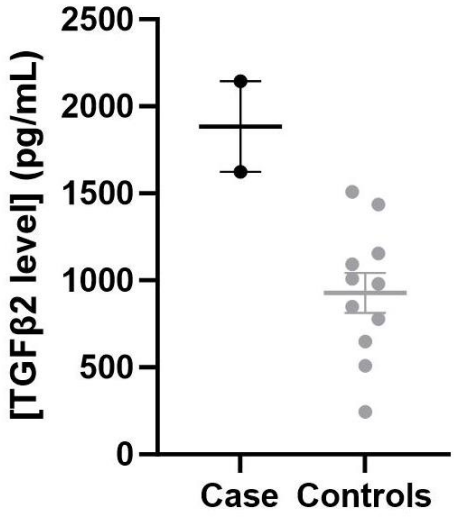

Figure 7. Analysis of TGFB2 concentration in the aqueous humor of a MCOR patient and controls. The ELISA dosage of TGFB2 in human samples reveals an accumulation of the protein in the MCOR patient analyzed, contrasting with 11 controls. Each data point on the graph represents the dosage value from the aqueous humor of an individual eye.